

Facile Synthesis of Fe-Doped Hydroxyapatite Nanoparticles from Waste Coal Ash: Fabrication of a Portable Sensor for the Sensitive and Selective Colorimetric Detection of Hydrogen Sulfide

Negar Alizadeh* and Abdollah Salimi



Cite This: *ACS Omega* 2022, 7, 42865–42871



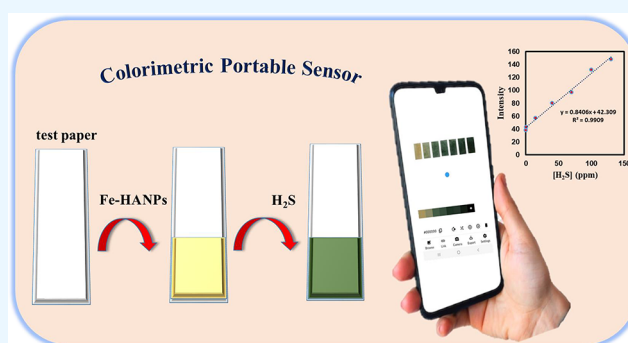
Read Online

ACCESS |

Metrics & More

Article Recommendations

ABSTRACT: In this work, a new strategy has been reported for the portable detection of H₂S based on Fe-doped hydroxyapatite nanoparticles (Fe-HA) using a colorimetric paper test strip integrated with a smartphone platform. Fe-HA NPs were fabricated successfully via recycling waste coal ash. The obtained probe response toward H₂S was through a distinct visual color change. The sensing mechanism is based on the displacement reaction, in which PO₄³⁻ is replaced by S²⁻. The prepared test strip shows high selectivity, and the other compounds containing thiol and sulfur anion have a negligible effect on the detection of H₂S. The designed scheme is applied for H₂S detection in the concentration range of 0.5–130 ppm with a limit of detection of 70 ppb. Furthermore, such a disposable sensor was used as a practical system for monitoring H₂S in actual water samples, suggesting the promising potential of this platform for suitable analysis of H₂S in an aqueous environment.



INTRODUCTION

Owing to increasing population and lack of raw materials, numerous studies are acting on reusing industrial waste as a source for the synthesis of nanomaterials.^{1,2} Coal ash is a major byproduct of coal combustion produced in large quantities during the energy production in the power plants.³ This solid waste is mainly disposed of in lagoons and landfill, which lead to groundwater and soil pollution.⁴ In recent years, numerous works have been conducted to recycle coal ash including manufacturing cement and ceramics, geopolymers production, zeolite synthesis, and stabilizing soils.^{5–8} However, compared to the amount of waste ash generated, the recycling scale is still low.⁸ Thus, it is required to find more ways to exploit the potential applications of this byproduct. Recently, many efforts have been made to synthesize diverse nanomaterials from fly ash such as iron oxide,⁹ magnesium oxide,¹⁰ mesoporous nanosilica,¹¹ and carbon nanofiber.¹² Abdelbasir et al. synthesized nanocuprous oxide from waste electric cables for the electrochemical detection of dopamine.¹³ An electrochemical sensor was prepared by anchoring cuprous oxide nanoparticles to flexible graphene electrode. In another study, an aluminosilicate framework was prepared from agro-waste material and introduced as a substrate and hosting material for AuNi bimetallic nanoparticles.¹⁴ The aluminosilicate framework possesses large porosity and high specific surface area for the construction of a suitable catalyst. The designed

sensing material was efficiently used for non-enzymatic glucose detection. Green production methods of sensor fabrication with recovered waste material meet the urgent need for sustainable, low-cost, and facile sensors.

Biological reports have confirmed that H₂S plays a significant role in health and disease by regulating physiological processes in the heart, liver, nervous system, and kidneys.^{15–17} Therefore, abnormal level of H₂S is associated with several illnesses including diabetes, hypertension cardiovascular diseases.^{18–20} Accordingly, designing an effective sensor for sensitive and selective determination of H₂S is critical. Numerous conventional methods such as chromatography,²¹ electrochemistry,²² fluorescence,²³ and colorimetric detection²⁴ have been built for H₂S detection. Among them, the colorimetric sensor is powerful tool as a detection platform due to its high sensitivity, excellent selectivity, and simple design without requiring a power source.^{25–27} Several colorimetric sensors have been employed for H₂S analysis based on organic dyes and or plasmonic metal nanoparticles.^{28,29} While these

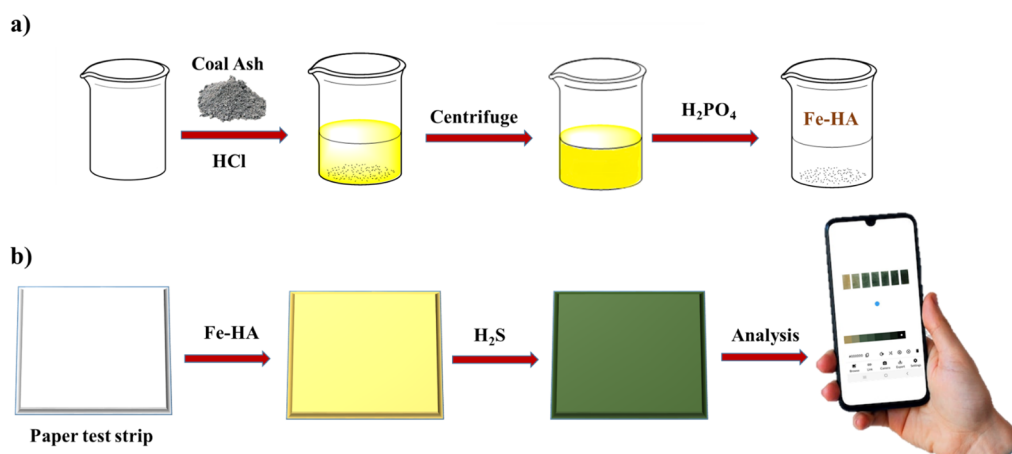
Received: August 2, 2022

Accepted: November 1, 2022

Published: November 16, 2022



Scheme 1. Schematic Illustration of (a) the Synthetic Process of Fe-Doped HA Nanoparticles and (b) the Colorimetric Detection of H₂S Using Fe-Doped HA Nanoparticles



detection techniques are accurate and sensitive, but, the application of those methods is hindered because they mostly rely on liquid media.³⁰

Lead acetate paper is a commercial sensor widely used for the colorimetric detection of H₂S. Upon the addition of H₂S, the white paper turns black from the formation of PbS.^{31,32} Over other analytical methods, paper test strips have rapidly developed in different areas because of low-cost and easy-to-use analytical tools.³³ Although this commercial test strip is popular and readily available, it has various drawbacks including the toxicity of lead metal and high detection limit.³⁴ Hence, a sensitive and green probe for the colorimetric detection of H₂S in the solid phase is highly desirable. Hydroxyapatite [Ca₁₀(PO₄)₆(OH)₂, HA] is an excellent biocompatible and low toxic nanostructure and has gained greater attention for construction of sensors. For instance, HA has been used for the detection of glucose,³⁵ hydrogen peroxide,³⁶ carbon dioxide,³⁷ cyanide³⁸ and phenolic compounds.³⁹ However, HA has been not reported to date for the detection of H₂S.

Here, a very simple method is reported for the synthesis of Fe-HA nanoparticles to be used in colorimetric test strips for smartphone-based detection of H₂S. The application of smartphones as a portable color sensor for chemical analysis reduces the expense and simplifies the operation.⁴⁰ In the presence of H₂S, the color of the paper strip turned green. This obvious color change could be easily observed by the naked eyes and quantitatively monitored by the smartphone. The detection mechanism was proposed as a displacement reaction between PO₄³⁻ and S²⁻. In contrast to the neurotoxic commercial lead (II) acetate-based test papers, this nanomaterial is used due to its non-toxic properties. The sensing properties of the paper strips were examined against increasing H₂S concentration between 0.5 and 130 ppm with a LOD of 70 ppb. Furthermore, the experimental results of the selectivity test display that the colorimetric sensor is not affected by thiol-containing interferences. Considering these characteristics, this proposed sensor a simple, portable, and inexpensive qualitative detector of H₂S for practical applications.

2. EXPERIMENTAL SECTION

2.1. Materials and Instruments. Sodium sulfide hydrate (Na₂S · xH₂O), monosodium phosphate (NaH₂PO₄), and sodium hydroxide (NaOH) were analytical grades purchased

from Sigma-Aldrich. All solutions were supplied by deionized water from a Milli-Q Plus system (Millipore). Scanning electron microscopy (SEM) images were recorded on MIRA3 TESCAN HV: 20.0 kV (Czech Republic). X-ray diffraction (XRD) patterns were acquired by a Bruker D8 Advance diffractometer using a copper source and a general area detector diffraction system (GADDS) (Netherlands). X-ray photoelectron spectroscopy (XPS) was obtained by a Kratos AXIS Supra spectrometer equipped with a monochromatic Al K (alpha) source (15 mA, 15 kV). The FT-IR spectra were recorded by a SPECTROD 250-Analytik Jena spectrophotometer (Germany).

2.2. Synthesis of Fe-HA Nanoparticles. The coal ashes received from the power plant were used as a precursor for the preparation of Fe-HA NPs (Scheme 1a). Ca²⁺ and (PO₄)³⁻ ions arranged around the OH⁻ ion in a hexagonal crystal structure. 10 calcium cations decorated in two non-equivalent positions with relative abundance of Ca(I)/Ca(II) = 2/3 and surrounded by phosphates. This arrangement in hexagonal unit cells makes HA a stable and flexible structure for cation substitution.⁴¹ Iron-substituted HA was synthesized by a facile method at room temperature. First, 1.0 g of coal ash was dispersed in 3 mL of water and then 3 mL of HCl was added as the leaching agent. The coal ashes contain high concentrations of metallic cations, particularly Ca²⁺ and Fe³⁺. The mixed slurry was stirred at 60 °C for 1 h. After leaching, the sample was centrifuged and the liquid phase was separated. Here, 20 mL of NaH₂PO₄ solution (0.5 M, pH = 10) was slowly added to the leachate taken to precipitate out the cations. After vigorous stirring for 15 min, the mixture was washed with deionized water several times. Finally, the precipitate product was dried and stored for further analysis.

2.3. Procedure for Colorimetric Studies. The stock solution of Fe-HA NPs (3 mM) was prepared in deionized water. A sheet of filter paper was cut into 2 × 1 pieces, and each piece was immersed in Fe-HA aqueous solution. The colorimetric tests were performed by dropping different concentrations of Na₂S aqueous solutions on paper strips. Afterward, a photograph was taken with the smartphone (Galaxy A31) and the green color intensity of each piece was measured using Color Picker application installed on the smartphone. The registered color intensity of papers was utilized to make the calibration curve which defines the analytical performance of the designed sensor.

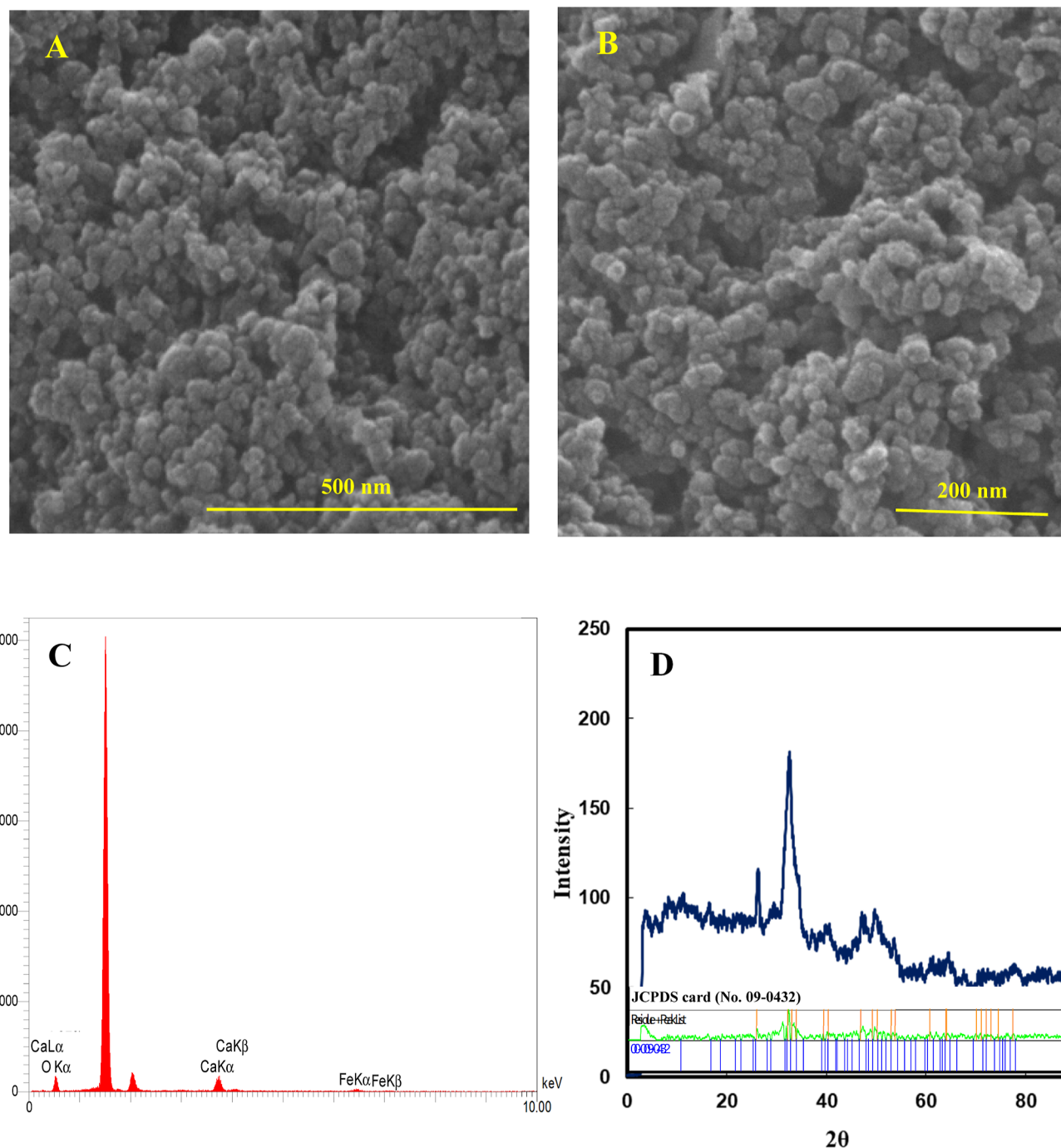


Figure 1. (A,B) SEM images and (C) EDS and (D) XRD pattern of Fe-doped HA nanoparticles.

For real sample analysis, the water samples of the tap water and river used to prepare Na_2S solution. After filtering, samples were spiked with different concentrations of Na_2S solution. The color intensity of all samples was recorded, and concentrations were calculated using the standard curve method.

3. RESULTS AND DISCUSSION

3.1. Characterization of Fe-HA NPs. To identify the structure of the Fe-HA nanocomposites, the SEM image is presented in Figure 1 A, B. The EDS analysis presented the atomic compositions of the prepared Fe-HA NPs in Figure 1C. The result reveals that the Fe/Ca atomic ratio value is 0.57. It

displays spherical morphology and an average size of about 20 nm. Powder XRD patterns were recorded over a 2θ range between 20 and 60° . As shown in Figure 1 D, the XRD peaks showed that the system crystallizes in the hexagonal $P6_3/m$ HA structure, matching the standard JCPDS card (no. 09–0432).⁴² No signals were observed related to metallic iron or iron oxide phases. The XPS spectra of the Fe-HA are shown in Figure 2, with Ca 2p, O 1s, and P 2p signals at 348, 531, and 135 eV, respectively. The chemical state of Ca, O, and P elements are accordance with the previous reports.^{43,44} The binding energies at 707 and 720.6 eV with an energy difference of 13.5 eV are attributed to Fe 2p $_{3/2}$ and Fe 2p $_{1/2}$, corresponding to the +3 oxidation state.⁴⁵ The FTIR graph

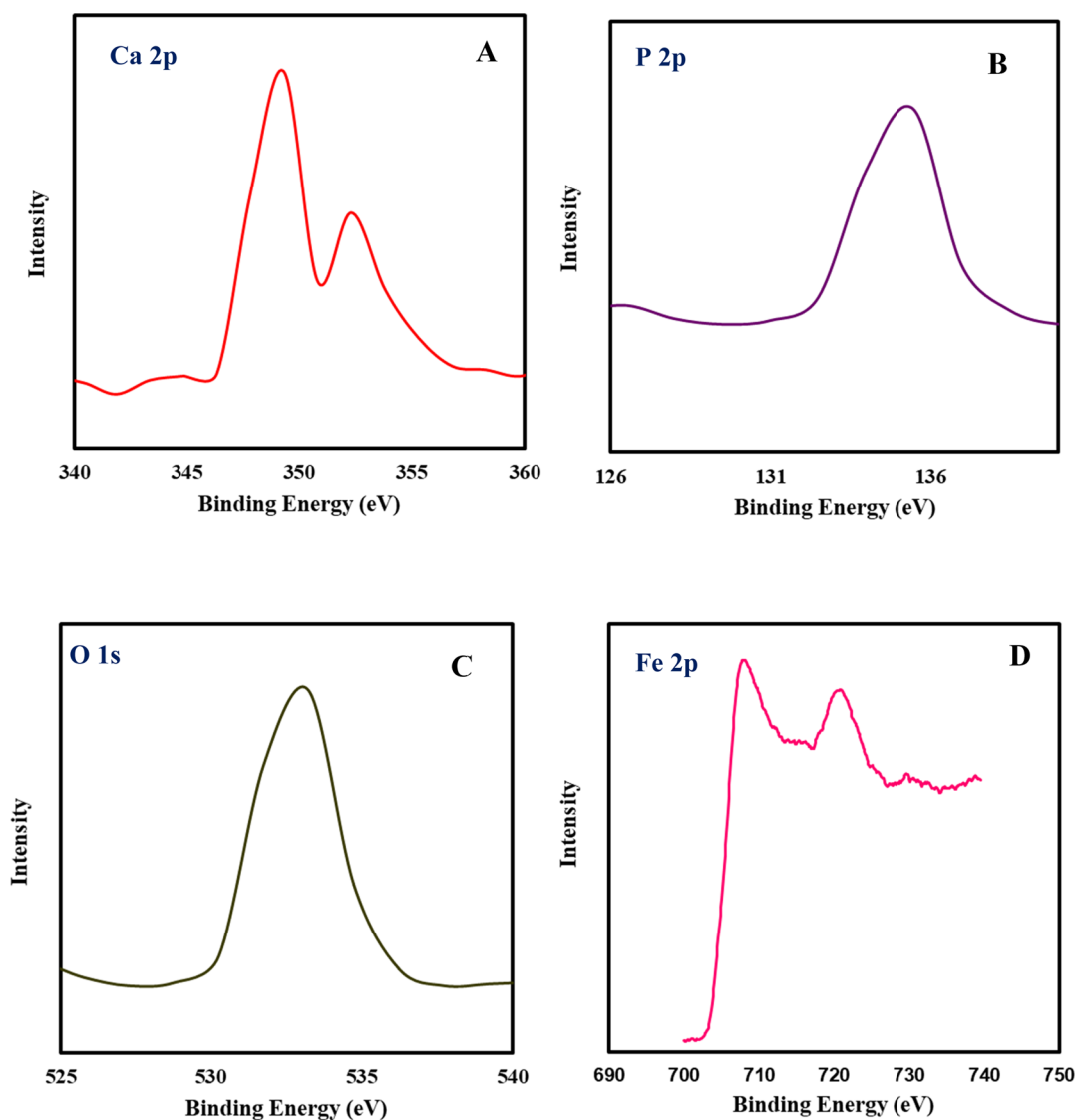


Figure 2. (A) Ca 2p, (B) P 2p, (C) O 1s, and (D) Fe 2p XPS spectra of Fe-doped HA nanoparticles.

of Fe-HA was recorded and shown in Figure 3. A broad peak between 3250 and 3450 illustrated the presence of adsorbed water molecules in the Fe-HA. The bands at 663 and 3550 cm^{-1} referred to the bending (ν_1) and stretching (ν_s)

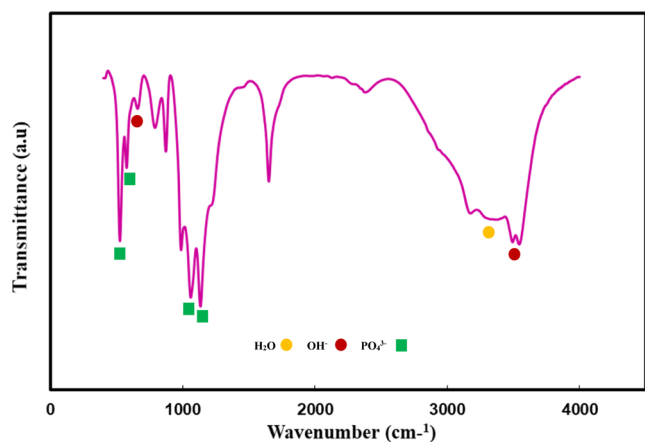
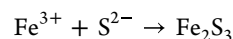


Figure 3. FTIR spectra of Fe-doped HA nanoparticles.

vibrational modes of the OH^- group, respectively. Peaks at 524 and 676 cm^{-1} were due to the triply degenerated (ν_4) bending modes of O–P–O phosphate bonds. The bands at 1060 and 1134 cm^{-1} were due to the triply degenerated (ν_3) asymmetric stretching mode of the P–O bonds.^{42,46}

3.2. Colorimetric Detection of H_2S by Fe-HA NPs. The colorimetric behavior of Fe-HA NPs was evaluated on the test strip by naked-eye detection and smartphone. Upon H_2S addition, the color of the test strip turned from yellow to green (Scheme 1b).

The detection mechanism is based on the replacement of PO_4^{3-} by S^{2-} and the formation of the Fe_2S_3 product. The green solid of Fe_2S_3 produced as follows



As seen in Figure 4A, with the increase in H_2S concentration, the probe response increased. The curves of the dynamic response of the Fe-HA NP sensor indicated nearly linear increase from 0.5 ppm to 130 ppm. The detection limit was measured as low as 70 ppb in aqueous solution. In comparison with other previously sensing platform for detection of H_2S , the proposed assay had a wide linear range

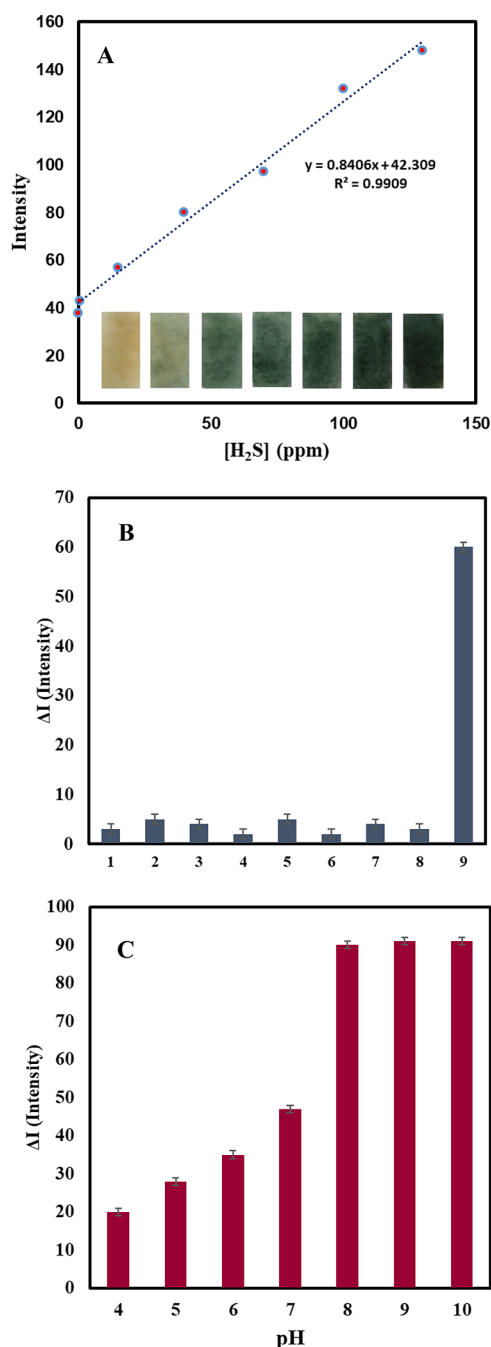


Figure 4. (A) Colorimetric response of the sensor to various concentrations of H_2S analyzed by the smartphone: (a) 0.5, (b) 15, (c) 40, (d) 70, (e) 100, and (f) 130 (ppm). (B) Selectivity of the proposed sensor toward different interferences including (1) $\text{Na}_2\text{S}_2\text{O}_3$, (2) GSH, (3) L-cysteine, (4) N-cysteine, (5) $\text{Na}_2\text{S}_2\text{O}_8$, (6) Na_2SO_4 , (7) NaSCN, (8) methionine, and (9) H_2S and (C) the effect of pH water toward Fe-doped HA response.

and low detection limit, which confirms the good potential of this method for the sensing of H_2S (Table 1).

In order to investigate the selectivity of the colorimetric sensor for the detection of H_2S , competitive species (GSH, cysteine, ...) were dropped onto the paper sensor platform to observe the color intensity changes under the same conditions. Figure 4B showed that, all interference compounds of the 10-fold concentration had no effect on the colorimetric sensor.

Table 1. Comparison of the Sensing Properties of Fe-Doped HA NPs with Other Sensors for the Detection of H_2S

sensing material	linear range (ppm)	detection limit (ppm)	reference
ZnO/CuO	1–20	1	48
Dye-loaded nanofiber	1–5	1	49
CuO–NiO	10–100	10	50
TiO ₂ –Fe ₂ O ₃	1–200	1	51
ZnFe ₂ O ₄	1–50	0.5	52
MWCNTs–COOH	up to 16	0.3	53
Fe-doped HA NPs	0.5–130	0.07	this work

Therefore, Fe-HA NPs would be appropriate for the detecting of H_2S in complex samples.

The practical applications of Fe-HA NPs were checked on the test papers. To this end, a paper sensor was prepared by immersing a filter paper in the Fe-HA NP solution. When the filter paper dried, river water with different concentrations of H_2S was dripped on the Fe-HA NPs@test paper. As can be seen in Table 2, the recovery and RSD ranges were 97–103.5%

Table 2. Detection of H_2S in Real Water Samples

samples	Spiked(ppm)	Measured(ppm)	Recovery(%)	RSD(%)
tap water	2	1.95	97	1.8
	10	10.11	101.1	2.6
	50	50.20	100.4	1.1
river water	2	2.07	103.5	0.9
	10	10.08	100.8	2.3
	50	50.56	101.1	1.7

and 0.9–2.6%, respectively, indicating the excellent potential of this colorimetric method for H_2S detection in real water samples. Furthermore, the colorimetric response of Fe-HA NPs for H_2S detection was also tested in various pH solutions (Figure 4C). It can be seen that in the presence of H_2S , the color change of Fe-HA was increased with the rise of pH level and reached a maximum at pH 8. These results indicated that alkaline reaction condition is better for the formation of iron sulfide.⁴⁷

4. CONCLUSIONS

In summary, for the first time, Fe-HA NPs were successfully synthesized from coal ash by a simple method. The synthesized Fe-HA NPs were applied for the fabrication of a novel colorimetric paper-based platform for specific detection of H_2S . The interaction between H_2S and Fe-HA NPs on colorimetric paper strips makes a color change from yellow to green. The sensing mechanism was on the basis of the anion replacement reaction between Fe-HA and H_2S . Quantitative detection of H_2S on the colorimetric paper test strip obtained from a smartphone application (Color picker). With the increase of H_2S concentration (0.5–130 ppm), the colorimetric response of Fe-HA NPs was gradually increased, and the LOD was obtained as 70 ppb. Furthermore, this colorimetric sensor applies to monitoring H_2S in environmental real samples. Taken together, the developed paper sensor integrated with the smartphone, provide simple, low cost, portable, and easy operation strategy for on-site detection of H_2S .

AUTHOR INFORMATION

Corresponding Author

Negar Alizadeh – Department of Chemistry, University of Kurdistan, Sanandaj 66177-15175, Iran; orcid.org/0000-0002-4046-6310; Phone: +9887336624001; Email: negaralizadeh310@yahoo.com

Author

Abdollah Salimi – Department of Chemistry, University of Kurdistan, Sanandaj 66177-15175, Iran; Research Center for Nanotechnology, University of Kurdistan, Sanandaj 66177-15175, Iran

Complete contact information is available at:
<https://pubs.acs.org/10.1021/acsomega.2c04905>

Notes

The authors declare no competing financial interest.

ACKNOWLEDGMENTS

The authors acknowledge financial support from the Research Office of University of Kurdistan (grant number 4.1261) and Iranian Nanotechnology Initiative Funds for research on microfluidic-based sensors.

REFERENCES

- (1) Beltrao-Nunes, A.-P.; Sennour, R.; Arus, V.-A.; Anoma, S.; Pires, M.; Bouazizi, N.; Roy, R.; Azzouz, A. CO₂ capture by coal ash-derived zeolites-roles of the intrinsic basicity and hydrophilic character. *J. Alloys Compd.* **2019**, *778*, 866–877.
- (2) Collins, F.; Rozhkovskaya, A.; Outram, J. G.; Millar, G. J. A critical review of waste resources, synthesis, and applications for Zeolite LTA. *Microporous Mesoporous Mater.* **2020**, *291*, 109667.
- (3) Pedrolo, D. R. S.; de Menezes Quines, L. K.; de Souza, G.; Marcilio, N. R. Synthesis of zeolites from Brazilian coal ash and its application in SO₂ adsorption. *J. Environ. Chem. Eng.* **2017**, *5*, 4788–4794.
- (4) Lee, Y.-R.; Soe, J. T.; Zhang, S.; Ahn, J.-W.; Park, M. B.; Ahn, W.-S. Synthesis of nanoporous materials via recycling coal fly ash and other solid wastes: A mini review. *Chem. Eng. J.* **2017**, *317*, 821–843.
- (5) Ahmaruzzaman, M. A review on the utilization of fly ash. *Prog. Energy Combust. Sci.* **2010**, *36*, 327–363.
- (6) Lee, J.; Lee, Y. H.; Jones, K.; Sharek, E.; Pascall, M. A. Antimicrobial packaging of raw beef, pork and turkey using silver-zeolite incorporated into the material. *Int. J. Food Sci. Technol.* **2011**, *46*, 2382–2386.
- (7) Andini, S.; Cioffi, R.; Colangelo, F.; Grieco, T.; Montagnaro, F.; Santoro, L. Coal fly ash as raw material for the manufacture of geopolymer-based products. *Waste management* **2008**, *28*, 416–423.
- (8) Kumpiene, J.; Lagerkvist, A.; Maurice, C. Stabilization of Pb- and Cu-contaminated soil using coal fly ash and peat. *Environ. Pollut.* **2007**, *145*, 365–373.
- (9) Qian, B.; Liu, C.; Lu, J.; Jian, M.; Hu, X.; Zhou, S.; Hosseini, T.; Etschmann, B.; Zhang, X.; Wang, H.; Zhang, L. Synthesis of in-situ Al³⁺-defected iron oxide nanoflakes from coal ash: A detailed study on the structure, evolution mechanism and application to water remediation. *J. Hazard. Mater.* **2020**, *395*, 122696.
- (10) Qian, B.; Hosseini, T.; Zhang, X.; Liu, Y.; Wang, H.; Zhang, L. Coal waste to two-dimensional materials: Fabrication of α -Fe₂O₃ nanosheets and MgO nanosheets from brown coal fly ash. *ACS Sustainable Chem. Eng.* **2018**, *6*, 15982–15987.
- (11) Yan, F.; Jiang, J.; Tian, S.; Liu, Z.; Shi, J.; Li, K.; Chen, X.; Xu, Y. A green and facile synthesis of ordered mesoporous nanosilica using coal fly ash. *ACS Sustainable Chem. Eng.* **2016**, *4*, 4654–4661.
- (12) Hintsho, N.; Shaikjee, A.; Masenda, H.; Naidoo, D.; Billing, D.; Franklyn, P.; Durbach, S. Direct synthesis of carbon nanofibers from South African coal fly ash. *Nanoscale research letters* **2014**, *9*, 387–11.
- (13) Abdelbasir, S.; El-Sheikh, S.; Morgan, V.; Schmidt, H.; Casso-Hartmann, L.; Vanegas, D.; Velez-Torres, I.; McLamore, E. Graphene-anchored cuprous oxide nanoparticles from waste electric cables for electrochemical sensing. *ACS Sustainable Chem. Eng.* **2018**, *6*, 12176–12186.
- (14) Amiripour, F.; Ghasemi, S.; Azizi, S. N. A novel non-enzymatic glucose sensor based on gold-nickel bimetallic nanoparticles doped aluminosilicate framework prepared from agro-waste material. *Appl. Surf. Sci.* **2021**, *537*, 147827.
- (15) Szabó, C. Hydrogen sulphide and its therapeutic potential. *Nature reviews Drug discovery* **2007**, *6*, 917–935.
- (16) Wang, M.; Song, Y.; Mu, P.; Cai, X.; Lin, Y.; Chen, C.-L. Peptoid-based programmable 2d nanomaterial sensor for selective and sensitive detection of H₂S in live cells. *ACS Applied Bio Materials* **2020**, *3*, 6039–6048.
- (17) Wang, F.; Xu, G.; Gu, X.; Wang, Z.; Wang, Z.; Shi, B.; Lu, C.; Gong, X.; Zhao, C. Realizing highly chemoselective detection of H₂S in vitro and in vivo with fluorescent probes inside core-shell silica nanoparticles. *Biomaterials* **2018**, *159*, 82–90.
- (18) Stein, A.; Bailey, S. M. Redox biology of hydrogen sulfide: implications for physiology, pathophysiology, and pharmacology. *Redox biology* **2013**, *1*, 32–39.
- (19) Kimura, H. Metabolic turnover of hydrogen sulfide. *Frontiers in physiology* **2012**, *3*, 101.
- (20) Lin, X.; Lu, X.; Zhou, J.; Ren, H.; Dong, X.; Zhao, W.; Chen, Z. Instantaneous fluorescent probe for the specific detection of H₂S. *Spectrochim. Acta, Part A* **2019**, *213*, 416–422.
- (21) Koike, S.; Kawamura, K.; Kimura, Y.; Shibuya, N.; Kimura, H.; Ogasawara, Y. Analysis of endogenous H₂S and H₂Sn in mouse brain by high-performance liquid chromatography with fluorescence and tandem mass spectrometric detection. *Free Radical Biology and Medicine* **2017**, *113*, 355–362.
- (22) Wang, S.; Liu, X.; Zhang, M. Reduction of ammineruthenium (III) by sulfide enables in vivo electrochemical monitoring of free endogenous hydrogen sulfide. *Analytical chemistry* **2017**, *89*, 5382–5388.
- (23) Li, S.; Huo, F.; Yin, C. NIR fluorescent probe for dual-response viscosity and hydrogen sulfide and its application in Parkinson's disease model. *Dyes Pigm.* **2022**, *197*, 109825.
- (24) Jia, Y.; Guo, Y.; Wang, S.; Chen, W.; Zhang, J.; Zheng, W.; Jiang, X. Nanocrystalline cellulose mediated seed-growth for ultra-robust colorimetric detection of hydrogen sulfide. *Nanoscale* **2017**, *9*, 9811–9817.
- (25) Alizadeh, N.; Salimi, A.; Hallaj, R.; Fathi, F.; Soleimani, F. Ni-hemin metal–organic framework with highly efficient peroxidase catalytic activity: toward colorimetric cancer cell detection and targeted therapeutics. *Journal of nanobiotechnology* **2018**, *16*, 93–14.
- (26) Alizadeh, N.; Salimi, A.; Hallaj, R. Mimicking peroxidase activity of Co₂(OH)₂CO₃-CeO₂ nanocomposite for smartphone based detection of tumor marker using paper-based microfluidic immunodevice. *Talanta* **2018**, *189*, 100–110.
- (27) Alizadeh, N.; Salimi, A.; Sham, T.-K.; Bazylewski, P.; Fanchini, G.; Fathi, F.; Soleimani, F. Hierarchical Co(OH)₂/FeOOH/WO₃ ternary nanoflowers as a dual-function enzyme with pH-switchable peroxidase and catalase mimic activities for cancer cell detection and enhanced photodynamic therapy. *Chem. Eng. J.* **2021**, *417*, 129134.
- (28) Zhang, D.; Jin, W. Highly selective and sensitive colorimetric probe for hydrogen sulfide by a copper (II) complex of azo-dye based on chemosensing ensemble approach. *Spectrochimica Acta Part A: Molecular and Biomolecular Spectroscopy* **2012**, *90*, 35–39.
- (29) Zeng, J.; Li, M.; Liu, A.; Feng, F.; Zeng, T.; Duan, W.; Li, M.; Gong, M.; Wen, C. Y.; Yin, Y. Au/AgI dimeric nanoparticles for highly selective and sensitive colorimetric detection of hydrogen sulfide. *Adv. Funct. Mater.* **2018**, *28*, 1800515.
- (30) Rosolina, S. M.; Carpenter, T. S.; Xue, Z.-L. Bismuth-based, disposable sensor for the detection of hydrogen sulfide gas. *Analytical chemistry* **2016**, *88*, 1553–1558.
- (31) Lawrence, N. S.; Davis, J.; Compton, R. G. Analytical strategies for the detection of sulfide: a review. *Talanta* **2000**, *52*, 771–784.

- (32) Papanikolaou, N. C.; Hatzidaki, E. G.; Belivanis, S.; Tzanakakis, G. N.; Tsatsakis, A. M. Lead toxicity update. A brief review. *Medical science monitor* **2005**, *11*, RA329–36.
- (33) Nguyen, T.-T. T.; Huy, B. T.; Lee, Y.-I. Disposable colorimetric paper-based probe for the detection of amine-containing gases in aquatic sediments. *ACS omega* **2019**, *4*, 12665–12670.
- (34) Carpenter, T. S.; Rosolina, S. M.; Xue, Z.-L. Quantitative, colorimetric paper probe for hydrogen sulfide gas. *Sensors and Actuators B: Chemical* **2017**, *253*, 846–851.
- (35) Zhang, Q.; Chen, C.; Xie, Q.; Liu, P. Electrodeposition of a biocompatible hydroxyapatite matrix to immobilize glucose oxidase for sensitive glucose biosensing. *Microchim. Acta* **2009**, *165*, 223–229.
- (36) Wang, B.; Zhang, J.-J.; Pan, Z.-Y.; Tao, X.-Q.; Wang, H.-S. A novel hydrogen peroxide sensor based on the direct electron transfer of horseradish peroxidase immobilized on silica–hydroxyapatite hybrid film. *Biosensors and Bioelectronics* **2009**, *24*, 1141–1145.
- (37) Mene, R. U.; Mahabole, M. P.; Khairnar, R. S. Surface modified hydroxyapatite thick films for CO₂ gas sensing application: Effect of swift heavy ion irradiation. *Radiat. Phys. Chem.* **2011**, *80*, 682–687.
- (38) Wang, S.; Lei, Y.; Zhang, Y.; Tang, J.; Shen, G.; Yu, R. Hydroxyapatite nanoarray-based cyanide biosensor. *Analytical biochemistry* **2010**, *398*, 191–197.
- (39) Lu, L.; Zhang, L.; Zhang, X.; Huan, S.; Shen, G.; Yu, R. A novel tyrosinase biosensor based on hydroxyapatite–chitosan nanocomposite for the detection of phenolic compounds. *Analytica chimica acta* **2010**, *665*, 146–151.
- (40) Feng, W.; Wan, Z.; Daniels, J.; Li, Z.; Xiao, G.; Yu, J.; Xu, D.; Guo, H.; Zhang, D.; May, E. F.; Li, G. Synthesis of high quality zeolites from coal fly ash: Mobility of hazardous elements and environmental applications. *Journal of Cleaner Production* **2018**, *202*, 390–400.
- (41) Carrera, K.; Huerta, V.; Orozco, V.; Matutes, J.; Fernández, P.; Graeve, O.; Herrera, M. Formation of vacancy point-defects in hydroxyapatite nanobelts by selective incorporation of Fe³⁺ ions in Ca (II) sites. A CL and XPS study. *Materials Science and Engineering: B* **2021**, *271*, 115308.
- (42) Jose, S.; Senthilkumar, M.; Elayaraja, K.; Haris, M.; George, A.; Raj, A. D.; Sundaram, S. J.; Bashir, A.; Maaza, M.; Kaviyarasu, K. Preparation and characterization of Fe doped n-hydroxyapatite for biomedical application. *Surfaces and Interfaces* **2021**, *25*, 101185.
- (43) Chang, M. C.; Tanaka, J. XPS study for the microstructure development of hydroxyapatite–collagen nanocomposites cross-linked using glutaraldehyde. *Biomaterials* **2002**, *23*, 3879–3885.
- (44) Kaciulis, S.; Mattogno, G.; Pandolfi, L.; Cavalli, M.; Gnappi, G.; Montenero, A. XPS study of apatite-based coatings prepared by sol-gel technique. *Appl. Surf. Sci.* **1999**, *151*, 1–5.
- (45) Hou, C.-H.; Hou, S.-M.; Hsueh, Y.-S.; Lin, J.; Wu, H.-C.; Lin, F.-H. The in vivo performance of biomagnetic hydroxyapatite nanoparticles in cancer hyperthermia therapy. *Biomaterials* **2009**, *30*, 3956–60.
- (46) Balakrishnan, S.; Padmanabhan, V. P.; Kulandaivelu, R.; Sankara Narayanan Nellaippan, T. S. N.; Sagadevan, S.; Paiman, S.; Mohammad, F.; Al-Lohedan, H. A.; Obulapuram, P. K.; Oh, W. C. Influence of iron doping towards the physicochemical and biological characteristics of hydroxyapatite. *Ceram. Int.* **2021**, *47*, 5061–5070.
- (47) Douglas, T.; Dickson, D. P.; Betteridge, S.; Charnock, J.; Garner, C. D.; Mann, S. Synthesis and structure of an iron (III) sulfide-ferritin bioinorganic nanocomposite. *Science* **1995**, *269*, 54–57.
- (48) Li, D.; Qin, L.; Zhao, P.; Zhang, Y.; Liu, D.; Liu, F.; Kang, B.; Wang, Y.; Song, H.; Zhang, T.; Lu, G. Preparation and gas-sensing performances of ZnO/CuO rough nanotubular arrays for low-working temperature H₂S detection. *Sensors and Actuators B: Chemical* **2018**, *254*, 834–841.
- (49) Kim, D.-H.; Cha, J.-H.; Lim, J. Y.; Bae, J.; Lee, W.; Yoon, K. R.; Kim, C.; Jang, J.-S.; Hwang, W.; Kim, I.-D. Colorimetric dye-loaded nanofiber yarn: Eye-readable and weavable gas sensing platform. *ACS Nano* **2020**, *14*, 16907–16918.
- (50) Wang, Y.; Qu, F.; Liu, J.; Wang, Y.; Zhou, J.; Ruan, S. Enhanced H₂S sensing characteristics of CuO–NiO core-shell microspheres sensors. *Sensors and Actuators B: Chemical* **2015**, *209*, 515–523.
- (51) Kheel, H.; Sun, G.-J.; Lee, J. K.; Lee, S.; Dwivedi, R. P.; Lee, C. Enhanced H₂S sensing performance of TiO₂-decorated α -Fe₂O₃ nanorod sensors. *Ceram. Int.* **2016**, *42*, 18597–18604.
- (52) Gao, X.; Sun, Y.; Zhu, C.; Li, C.; Ouyang, Q.; Chen, Y. Highly sensitive and selective H₂S sensor based on porous ZnFe₂O₄ nanosheets. *Sensors and Actuators B: Chemical* **2017**, *246*, 662–672.
- (53) Parsafar, N.; Ghafouri, V.; Banaei, A. Electrochemical sensing of H₂S gas in air by carboxylated multi-walled carbon nanotubes. *Iranian Journal of Chemistry and Chemical Engineering (IJCCE)* **2019**, *38*, 53–62.